atmosphere

MDPI

Article

Effects of Horizontal Transport and Vertical Mixing on Nocturnal Ozone Pollution in the Pearl River Delta

Honglong Yang [1], Chao Lu [1], Yuanyuan Hu [1], Pak-Wai Chan [2], Lei Li [3,*] and Li Zhang [1]

[1] Shenzhen National Climate Observatory, Meteorological Bureau of Shenzhen Municipality, Shenzhen 518040, China
[2] Hong Kong Observatory, Hong Kong 999077, China
[3] School of Atmospheric Sciences, Sun Yat-sen University, Zhuhai 519082, China
* Correspondence: lilei68@mail.sysu.edu.cn

Abstract: Based on the meteorological, ozone (O_3), and vertical observation data of 2020, this study sought to evaluate the daily variation in O_3, particularly the characteristics of nocturnal ozone pollution. We also discuss the effect of local and mesoscale horizontal transport and vertical mixing on the formation of nocturnal O_3 pollution. Distinct seasonal characteristics of the daily O_3 variation in Shenzhen were identified. In particular, significant nocturnal peaks were found to regularly occur in the winter and spring (November–December and January–April). The monthly average of daily variation had a clear bimodal distribution. During the period, O_3 pollution frequently occurred at night, with the maximum hourly O_3 concentration reaching 203.5 $\mu g/m^3$. Nocturnal O_3 pollution was closely associated with horizontal transport and vertical mixing. During the study period, the O_3 maximum values were recorded on 68 nights, primarily between 23:00 and 03:00, with occasional observation of two peaks. The impact of horizontal transport and vertical mixing on the nocturnal secondary O_3 maximum values was elaborated in two case studies, where vertical mixing was mainly associated with low-level jets, with strong wind shear enhancing turbulent mixing and transporting O_3 from the upper layers to the surface.

Keywords: secondary ozone maximum; advection; vertical mixing

Citation: Yang, H.; Lu, C.; Hu, Y.; Chan, P.-W.; Li, L.; Zhang, L. Effects of Horizontal Transport and Vertical Mixing on Nocturnal Ozone Pollution in the Pearl River Delta. *Atmosphere* **2022**, *13*, 1318. https://doi.org/10.3390/atmos13081318

Academic Editors: Riccardo Buccolieri, Jian Hang, Liyue Zeng and Cho Kwong Charlie Lam

Received: 29 July 2022
Accepted: 15 August 2022
Published: 18 August 2022

1. Introduction

Ground-level ozone (O_3) significantly harms human health and ecological conditions. The continued deterioration of atmospheric conditions due to O_3 pollution has become an environmental issue of major concern. Due to urbanization and industrialization, O_3 pollution has plagued many areas in China [1] and has become increasingly complex, with regional characteristics [1]. In some cities, O_3 concentrations are increased above the national standard approximately 20% of the time throughout the year. Further, in other areas, maximum hourly O_3 concentrations have exceeded the European O_3 alert threshold of 240 $\mu g/m^3$ [2–5]. O_3 and several other pollutants can cause severe illnesses, such as tracheitis and impaired lung functions, due to repeated exposure [6,7]. O_3 pollution can also cause a 10% decrease in the yields of major food crops (including wheat, rice, soybean, and potato) [8] and has impacts in various ecosystems [9]. Therefore, the current atmospheric O_3 pollution is a threat to human health and food security and causes ongoing damage.

O_3 pollution not only shows specific features varying with geographic location but also displays significant daily variations [10]. Under clear weather conditions, O_3 concentrations displayed significant daily variation, with maximum values appearing in the afternoon and minimums occurring from evening to early morning [11]. At night, there is no solar radiation or source of O_3. Nitrogen oxides (NO) emitted from local urban sources react with O_3 to produce nitrogen dioxide (NO_2), resulting in O_3 depletion. This, combined with efficient loss of O_3 through surface deposition, results in minimum O_3 concentrations during the late evening/early night. The daily O_3 variation pattern is almost the same in urban and

rural areas. However, high nighttime O_3 values have been observed in different parts of Europe, North America, South America, and several regions in Asia [12–16]. These observations have indicated clear nocturnal O_3 peaks, with concentrations exceeding 100 $\mu g/m^3$ at certain times. Within a stable nocturnal boundary layer, with no known sources of O_3 pollution and in the absence of photochemical processes, nocturnal O_3 concentrations can only be explained by meteorological conditions. High nocturnal O_3 concentrations are mainly explained by external transport and vertical mixing. For instance, Chung proposed that downward transport by vertical mixing is the primary cause of nighttime O_3 peaks [17]. Baumbach and Vogt's observations in Freiburg, Germany, suggested that local nighttime O_3 maximum values might be caused by valley breeze [18]. Recent numerical model sensitivity tests indicated that nocturnal low-level jets (LLJ) may cause cracks in the nocturnal residual layer (RL), resulting in high nighttime O_3 concentrations [19]. By performing an extensive literature review, Tong et al. [20] concluded that nocturnal O_3 pollution is a weak link in current O_3 research, and more research should be carried out to elucidate its formation and causes.

In recent years, O_3 pollution has gradually become a major concern in air pollution events in the Pearl River Delta (PRD) region. Favourable climatic conditions, combined with abundant VOCs and NOx emissions from natural and anthropogenic sources [21–23], have led to more serious O_3 pollution in the region. O_3 has gradually replaced $PM_{2.5}$ to become the dominant pollutant [24]. The maximum hourly O_3 concentration is 428–470 $\mu g/m^3$ [25], and long-term observation data revealed an uptrend in O_3 concentrations [26]. In this context, nocturnal O_3 pollution has attracted attention. However, due to limited observation data, existing studies have primarily focused on the processes and causes of daytime O_3 [27], with little attention to nocturnal O_3. Further, the limited studies were mainly case studies [28,29]. In this study, we analysed nocturnal O_3 maximums and meteorological data of 2020 for Shenzhen, a representative city in the PRD region, to investigate the extent, frequency, and time of nocturnal O_3 pollution and the impact of local and mesoscale weather systems on these factors. As a coastal city in southern China, Shenzhen is one of the three national financial hubs in China and the core city of the PRD metropolitan region. The city connects Hong Kong to mainland China and is surrounded by vast coastal sea area leading to the South China Sea and the Pacific Ocean. Due to the special geographical, topographical, and climatic characteristics of the region, pollution is influenced not only by sea and land breezes but also by regional weather systems and typhoons [30–32]. In previous decades, O_3 and other pollutants have been monitored in the Shenzhen area, and meteorological observations and studies have been sufficiently carried out [33,34]. Accordingly, the region is a good candidate for studying nocturnal O_3 and the impact of meteorological conditions on pollution.

2. Introduction to the Sampling Sites and Methodology

To analyse the frequency, level, and causes of O_3 pollution at night, we selected O_3 concentrations, meteorological data, and meteorology tower observations obtained in 2020. The distribution of stations is shown in Figure 1. Hourly O_3 concentrations were measured at the Zhuzilin monitoring station of the Shenzhen Meteorological Bureau (22°32′ N, 114°0′ E, with 63 m elevation) using a dual-cell, UV photometric Model 49i O_3 Analyser (ThermoFisher Scientific, Waltham, MA, USA) with a measurement range of 0–400 mg/m^3, minimum detection limit of 1 $\mu g/m^3$, zero drift of <2.14 $\mu g/m^3$/24 h, and response time of 20 s. The station is located next to the city park of Shenzhen, with primarily commercial, business, and residential areas and no industrial sources in the vicinity.

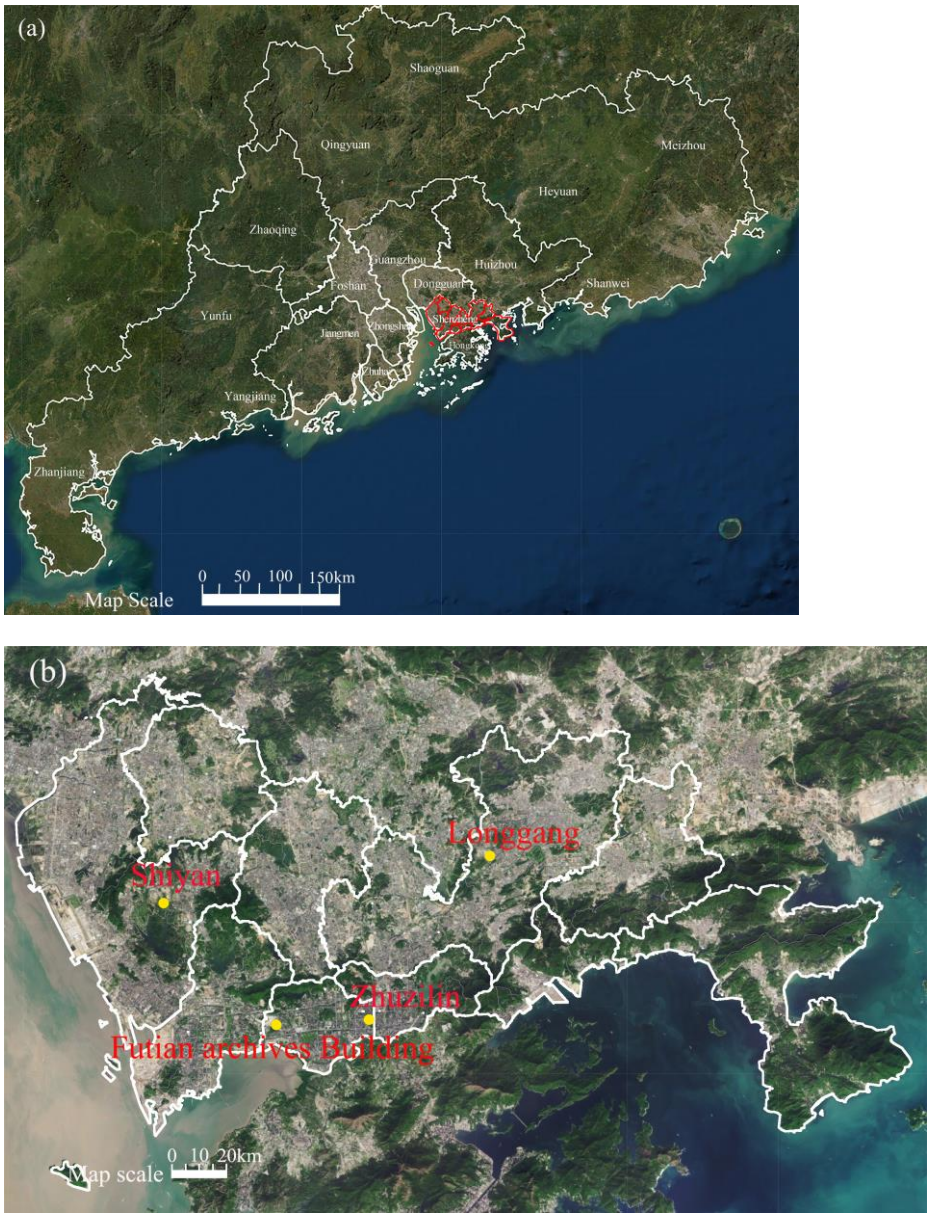

Figure 1. The geographical location of the Pearl River Delta region in China (**a**) and the research station in Shenzhen (**b**) (marked as yellow dot).

Meteorological observation data were recorded at the meteorology tower (Shiyan) and the automatic weather station (Zhuzilin) (Figure 1). The meteorology tower carried out observations (wind, temperature and humidity) at 13 levels using Vaisala equipment [33]. The wind profile observations were obtained from the Longgang observation base with Vaisala LAP-3000 equipment (Table 1). The vertical profiles of atmospheric O_3 concentration were observed by atmospheric ozone detection lidar on the Futian Archives building, with a spatial resolution of 30 m and an effective detection height larger than 3 km. The ERA5 atmospheric reanalysis data, including 950 hPa horizontal wind vectors and ozone mixing ratio, from the European Centre for Medium-Range Weather Forecasts (ECMWF), were collected hourly on 14 March 2020 with a horizontal resolution of $0.25° \times 0.25°$. All the data used in this paper were reported in Local Time (LT).

Table 1. Description of the equipment.

Parameter Measured	Measuring Levels (m)	Instrument	Accuracy	Observation Address
O_3	2 m	Thermo Scientific Model 49i	2 μg/m^3	Zhuzilin
Wind direction Wind speed	10 m	Vaisala WMT703	0.1 m/s	Zhuzilin
Wind direction Wind speed	10 m, 20 m, 40 m, 50, 80 m, 100 m, 150 m, 160 m, 200 m, 250 m, 300 m, 320 m, 350 m	Vaisala WMT703	0.1 m/s	Shiyan meteorology tower
Temperature		Vaisala HMP155	<0.2 °C	Shiyan meteorology tower
Wind profile	Max altitude: 3–6 km Vertical resolution: 60 m	Vaisala LAP-3000	≤1.5 m/s (RMS) ≤10° (RMS)	Longgang
Ultrasound wind	40 m	Campbell CSAT3	50 Hz U_x, U_y < ±0.08 m/s U_Z < ± 0.04 m/s	Shiyan meteorology tower
Ozone profile	Max altitude: 3 km Vertical resolution: 30 m	Wuxi Zhongke Optoelectronics Co., Ltd.	<6 μg/m^3	Futian Archives Building

According to the results of previous studies [17,35], nocturnal O_3 pollution generally occurred under stable atmospheric conditions. To select stable atmospheric conditions and avoid sudden weather clear-up, we selected the period from 3 h before sunset until sunrise with hourly average wind speeds of no more than 2 m/s. The data were collected from the ground automatic meteorological observation station (Zhuzilin in Figure 1). Vertical meteorological observation data from the meteorology tower at the Shiyan station were used to analyse atmospheric stability and the variability characteristics of the horizontal and vertical wind fields. Wind profile information was utilised to analyse low-level jets (LLJs). An LLJ is defined by Whiteman criteria [36], namely, that (1) the maximum wind speed is more than 10 m·s^{-1} in the lowest 3 km and (2) the wind speed must decrease by at least 5 m·s^{-1} from the height of the wind maximum to the wind minimum below a height of 3 km or to a height of 3 km when no minimum is found. Turbulent Kinetic Energy (TKE) is calculated using the data from 40 m three-dimensional ultrasonic anemometer. Atmospheric stability was assessed using the bulk Richardson number (Ri_b). Ri_b was calculated using temperatures and wind speeds from two layers [37], which were collected from the 10 m and 350 m meteorology towers in this study. Nocturnal O_3 pollution describes a process where the nighttime O_3 concentrations under stable conditions stop decreasing and instead increase by more than 10 μg/m^3 relative to the point of trend change.

3. Results and Discussion

3.1. General Characteristics of O_3

In 2020, the annual average concentration in Shenzhen was 65.5 μg/m^3, with a maximum hourly concentration of 348.9 μg/m^3. Although nighttime concentrations were relatively low, some high O_3 concentrations were observed at night, with a maximum hourly concentration of 203.5 μg/m^3. Figure 2 shows the daily variation in O_3 concentrations in each month in 2020. This variation reflects the seasonal changes in O_3 concentrations in Shenzhen, with the maximum recorded in autumn and the minimum recorded in summer. During the summer, the daily variation cycle showed a daytime maximum and a nighttime minimum. The daily variation in autumn was similar to that in summer, although a slight peak was observed during the concentration decrease around midnight. During the wintertime, a clear bimodal structure was observed, despite a markedly lower nighttime maximum relative to the daytime maximum. In spring, the daily variation in O_3 concentrations displayed a similar pattern to that in winter. During the study period, the highest

nighttime hourly O_3 concentration of 203.5 μg/m^3 appeared in April, and the nighttime maximum values gradually decreased from winter to summer. Similar daily O_3 variation cycles were observed in other regions, such as Montreal, Canada [17]; Portugal [38]; Hong Kong [39]; and Beirut, Lebanon [40]. Kulkarni et al. [41] discovered a bimodal structure for daily variations in ground-level O_3 concentrations in the UK during the wintertime; this structure was particularly pronounced between November and January, with nighttime maximums even higher than the daytime maximums. Saliba et al. [40] reported that the secondary ozone maximum is attributed to a regional source of ozone, but downward transport by vertical mixing is the physical interpretation, as suggested by Chung [17] and Leung et al. [39]. Corsmeier et al. [12] especially focus on the effect of enhanced mechanical turbulence produced by a LLJ. Zhu et al. [28] analysed the O_3 vertical distribution characteristics, and they illustrated that the atmospheric turbulence led to correlative variation characteristics of O_3 concentration in different heights. He et al. [29] show that synoptic processes such as convective storms and low-level jets can lead to the nocturnal ozone enhancement event by aggravating vertical mixing. Additionally, horizontal transport of ozone-rich plumes may also be a supplementary driver. The enhancement of nocturnal surface ozone is most likely associated with horizontal transport and low-level jets in this study, which will be described in detail later.

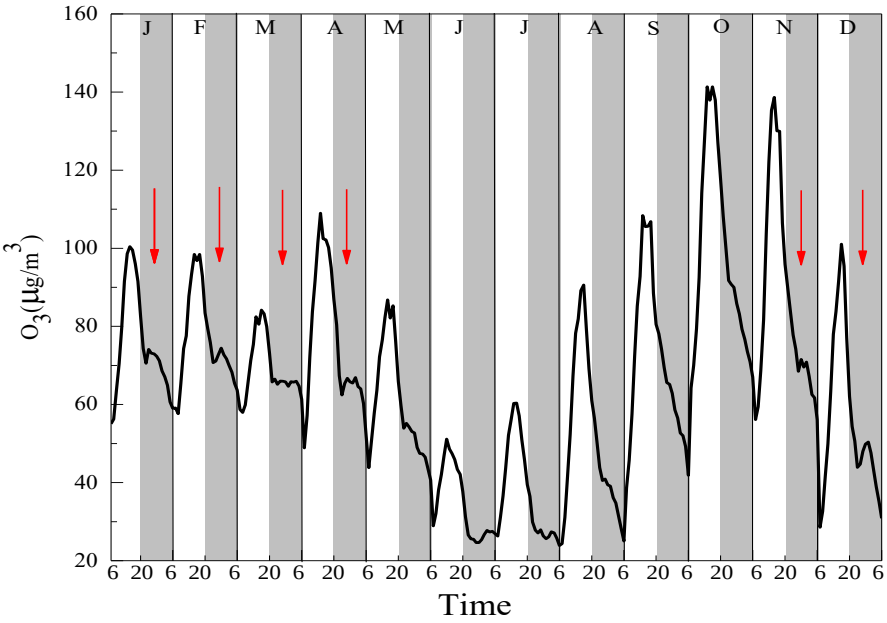

Figure 2. Daily variation in O_3 concentrations in individual months of 2020. Gray indicates nighttime.

3.2. Causes of Nighttime Ozone Maximums

To identify the possible causes of nighttime O_3 maximums, we analysed the features of nighttime O_3 during the 2020 observation period and found a total of 68 days with nighttime O_3 maximums. When the nighttime O_3 maximum occurred, the daily variation pattern of O_3 concentrations (Figure 3) displayed a clear bimodal structure, with the maximum peak appearing between 12:00 and 14:00 LT during the day and the secondary peak mainly occurring between 23:00 and 03:00 LT at night. Maximum nighttime O_3 concentrations ranged from 33.1 to 203.5 μg/m^3, with hourly average concentrations exceeding 80 μg/m^3 on 13 nights.

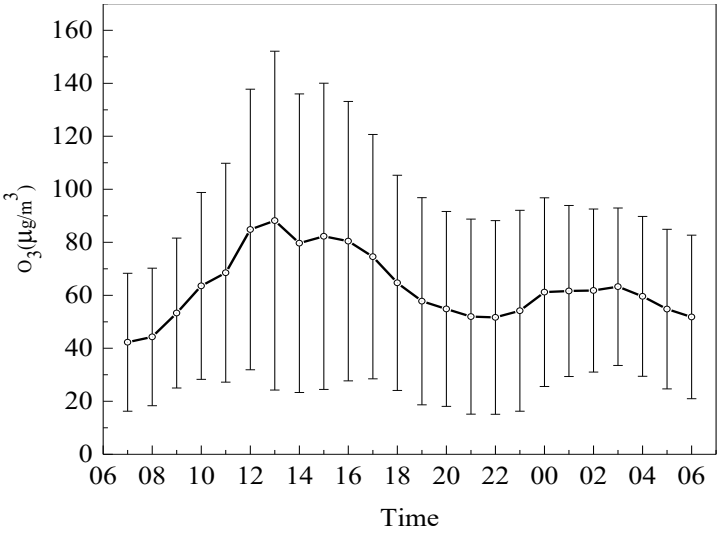

Figure 3. Corresponding daily variation in O_3 concentrations during the occurrence of nighttime O_3 maximums.

To investigate the causes of the nocturnal O_3 maximum, Eliasson et al. [42] proposed a method to analyse the role of horizontal transport and vertical mixing in the formation of nocturnal O_3 pollution based on various analytical methods. The method established three criteria to determine and differentiate the contribution of the two processes. All three conditions depicted in Table 2 should be satisfied to attribute the nighttime O_3 maximum to horizontal transport. On the contrary, if the second or the third criterion is not met, the nighttime O_3 pollution is caused by vertical mixing. Based on the three criteria listed in Table 2 and the meteorological conditions, we found that 30 of the 68 nighttime O_3 pollution incidents were caused by vertical mixing, which transported high concentrations of O_3 in the upper levels to the ground. Further, 16 events were caused by horizontal advection of O_3. Twenty-two days could not be clearly explained by horizontal and vertical mixing. However, it should be pointed out that the categories of cases identified by using the criteria in Table 2 are not completely convincing. For example, in some cases identified as vertical mixing ones, horizontal transportation actually made more important contribution. In fact, to accurately identify which process plays a major role in the formation of nocturnal ozone pollution, it is necessary to conduct in-depth analysis based on the observation data in the boundary layer, which is of great significance for further understanding the dynamic mechanism of nocturnal ozone concentration rise events. The analysis of the identified cases clearly revealed the important roles of local weather and vertical mixing in the formation of O_3 pollution at night. Two case studies were carried out to further elucidate the roles of horizontal and vertical processes in the nocturnal O_3 maximums.

Table 2. Criteria for nighttime O_3 pollution transport analysis.

No.	Horizontal Transport	Vertical Mixing
1	Average wind speed $\leq$ 2 m/s from 3 h before sunset to sunrise and atmosphere in stable stratification (bulk Richardson number (Ri_b) > 0)	
2	$Ri_b > 1$	$Ri_b < 1$
3	Wind direction at the beginning of or before the increase in O_3 concentration (W-NW to E-SE)	No change in wind direction during or before the increase in O_3 concentration

3.2.1. Origin of Nocturnal O_3 Events: Horizontal Transport

From 8 April to 9 April, the upper 500 hPa level in the Shenzhen area was controlled by westerly wind, the 850 hPa level existed in a weak ridge field, and the ground was

controlled by a weak high-pressure ridge, with poor dynamic conditions in the entire layer, stable weather, and weak wind. The observed hourly atmospheric O_3 concentration distribution is shown in Figure 4. At night, the O_3 concentration increased from 61.3 μg/m^3 to 107.5 μg/m^3 between 17:00 and 00:00, followed by a gradual decline to 44.8 μg/m^3 by 06:00. In order to understand whether horizontal advection or turbulent downward mixing caused an increase in nighttime O_3 concentration, turbulence was analysed, using Ri_b. The increase in ground-level O_3 was closely related to the increase in Ri_b, with Ri_b increasing from 0.6 at 16:00 to 9.9 at 21:00 (Figure 4a), indicating stable atmospheric stratification. During this time, vertical mixing was weak and horizontal transport was favoured. The rapid shift in surface wind direction from southerly to easterly–northeasterly served as additional evidence of horizontal transport in the atmosphere (Figure 4b). The change in surface wind direction was preceded by a rapid decline in wind speed from >1 m/s to approximately 0.4 m/s (Figure 4c). Wind speeds remained low throughout the night until the next morning (06:00), when the surface winds changed direction to southwesterly. The northeasterly winds are expected to transport the ozone-rich air in the sea to the Shenzhen, contributing to nocturnal ozone enhancement there. This is also supported by the backward trajectory analyses using the Hybrid Single-Particle Lagrangian Integrated Trajectory (HYSPLIT) model (Figure 5). Previous studies have indicated that the land breezes can transport the local pollutants in Shenzhen to the sea, and the sea breezes can transport the pollutants back to Shenzhen [43].

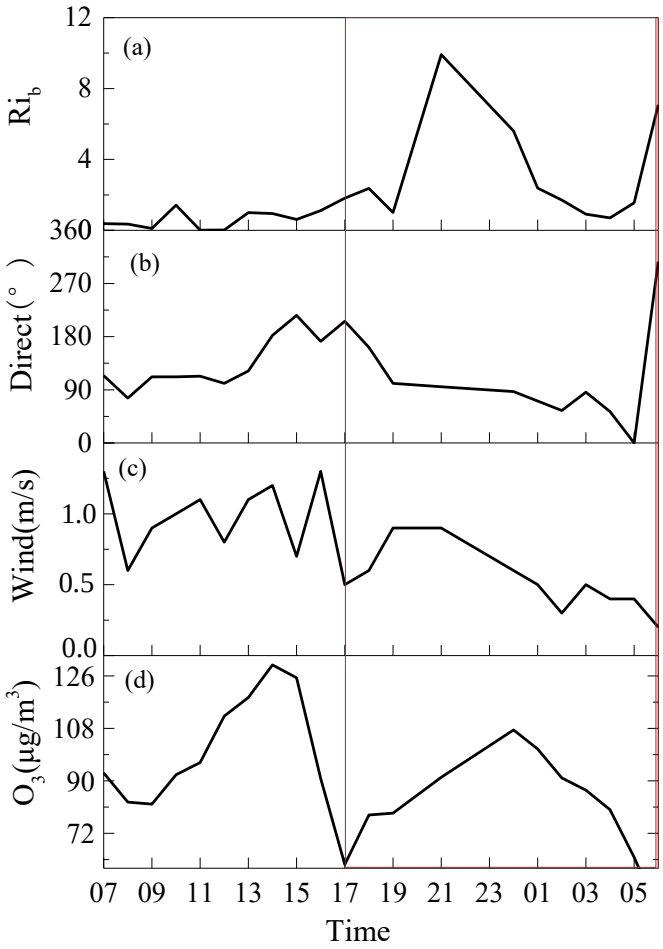

Figure 4. Characteristics of the variation in the bulk Richardson number (Ri_b) (**a**), wind direction (**b**), wind speed (**c**), and O_3 concentration (**d**) from 8 to 9 April 2020.

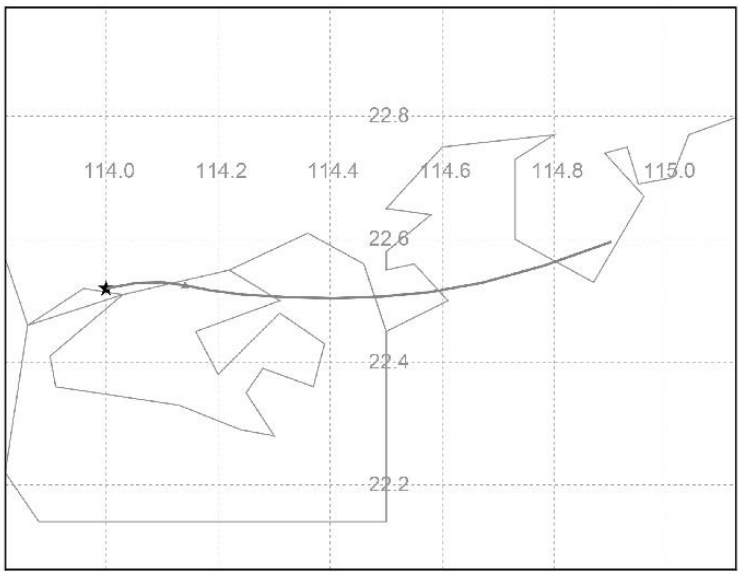

Figure 5. The 12 h backward trajectories of air mass calculated using the HYSPLIT model at 23:00, 8 April.

In summary, the increase in O_3 concentration during the night from 8 April to 9 April 2020 can be explained as follows: around sunset (17:00 LT), the near-surface air stabilized, wind speeds weakened, and chemical reactions alongside surface deposition reduced ozone concentrations. Under the stable atmospheric conditions, turbulent mixing was suppressed, and horizontal movement was promoted by the temperature differences between land and ocean and the northeasterly winds.

3.2.2. Origin of Nocturnal O_3 Events: Vertical Mixing

Figure 6a shows that the O_3 concentration during the nighttime between 00:00 and 06:00 on 14 March 2020 rose from 14 $\mu g/m^3$ to 40 $\mu g/m^3$. Figure 7 shows the spatial distribution of ozone concentration and horizontal wind vector at the 950 hpa level. It can be seen from Figure 7 that under the condition of the prevailing north wind, the air mass in the high O_3 area was gradually transported to seashore land during the period of 00:00 to 07:00 on 14 March. At the same time, a low–level jet occurred (Figure 6b), which further facilitated the O_3 inland to be transported to the coastal areas. A wind profiler radar recorded the evolution of the vertical profile of wind speed on the night of 14 March (Figure 6b), and an obvious low-level jet appeared during the period of 02:00 to 06:00. The maximum wind speed of the low-level jet was recorded at the height of 400–700 m, reaching 15 m/s. During this period, vertical mixing might have been enhanced within the surface layer due to the strong vertical shear of wind speed, resulting in an increase in surface O_3 concentration [18]. Based on this inference, the vertical distribution of O_3 concentration during this period was further analysed in Figure 6c. A significant decrease in O_3 concentration at 0.4–1.0 km and an increasing tendency in the lower atmospheric layers can be found, which indicates that the LLJ may enhance the vertical mixing of mass within the boundary layer. Furthermore, it can be seen from Figure 6d that the TKE within the surface layer increased rapidly from 02:00 to 07:00, reaching a maximum of 2.5 m^2/s^2, which was further evidence that the LLJ enhanced vertical turbulent mixing. Therefore, LLJs might promote the enhancement of vertical mixing and increase the ground-level O_3 concentration at night.

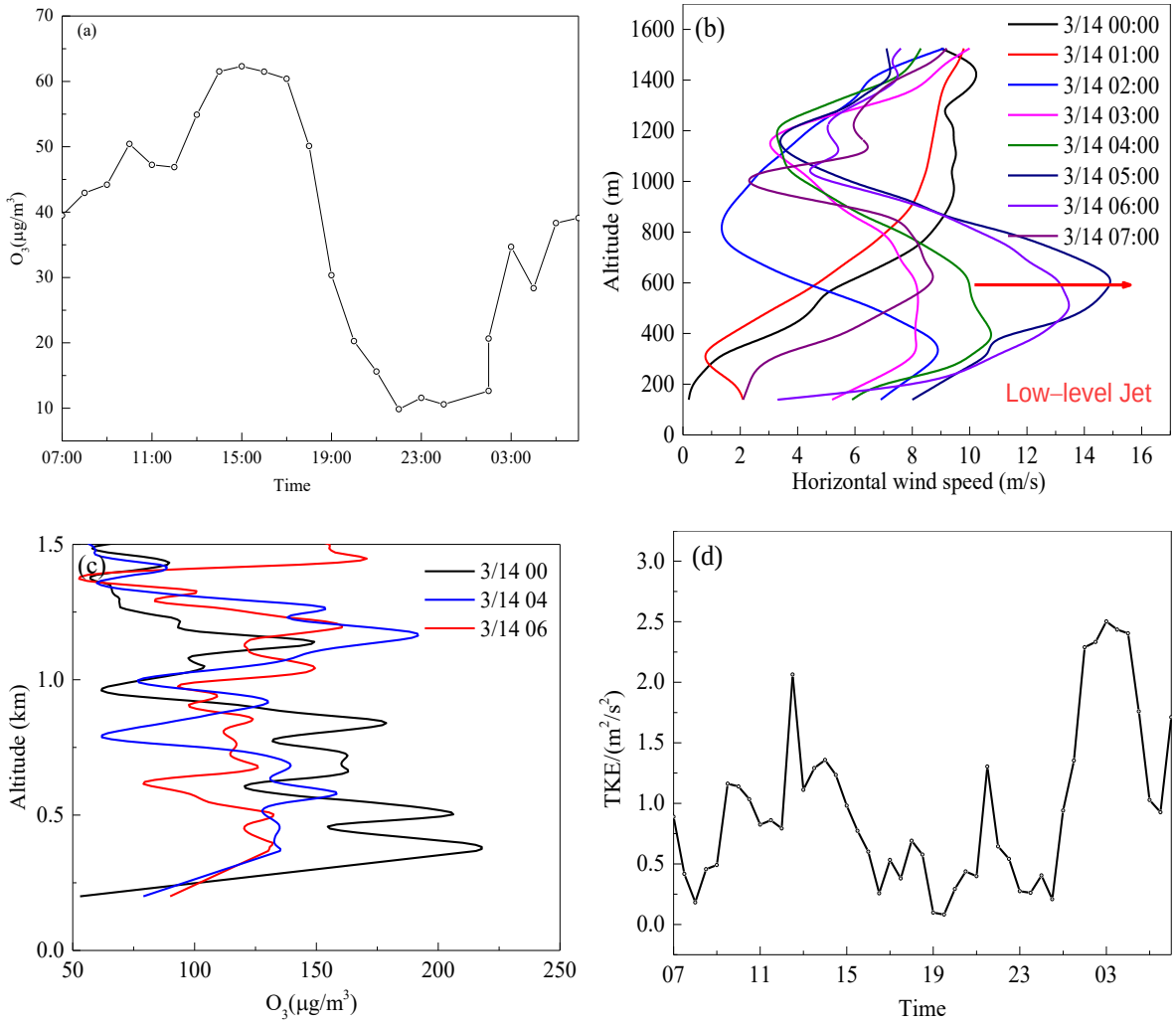

Figure 6. (**a**) Temporal change in hourly ozone concentration from 07:00 LT on 13 March to 06:00 LT on 14 March 2020; (**b**) Horizontal wind speed profiles from 00:00 to 06:00 LT on 14 March 2020, respectively; (**c**) Ozone concentration profiles at 00:00, 04:00, and 06:00 LT on 14 March 2020, respectively, which were observed by atmospheric ozone detection lidar on the Futian Archives building (indicated by black pentagram in Figure 7); (**d**) Characteristic variations in TKE at 40 m from the meteorology tower from 13 to 14 March 2020.

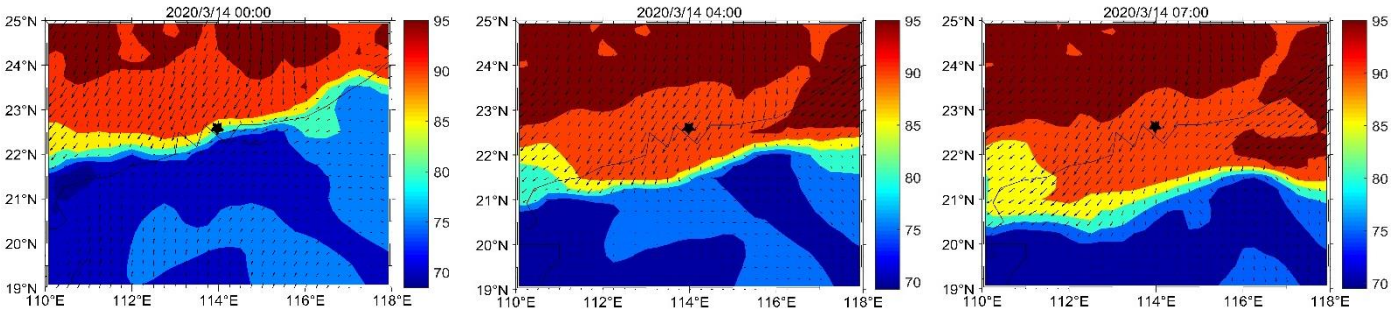

Figure 7. Geographical distribution of the composites of 950 hPa O_3 concentration (units: μg/m^3; shaded colours) and 950 hPa horizontal wind vectors at 00:00, 04:00, 07:00 on 14 March 2020, respectively (data from the ECMWF). The black pentagram is the location of the ozone profile.

Therefore, the entire night O_3 pollution event can be explained by Figure 8, during which the LLJ played an important role. In the horizontal direction, the LLJ efficiently

transported the inland airmass with rich O_3 to the coastal areas. At the same time, due to the strong vertical shear of wind speed caused by LLJ, the turbulence in the surface layer was enhanced, so that the O_3 at high altitudes was delivered to the ground through vertical exchange.

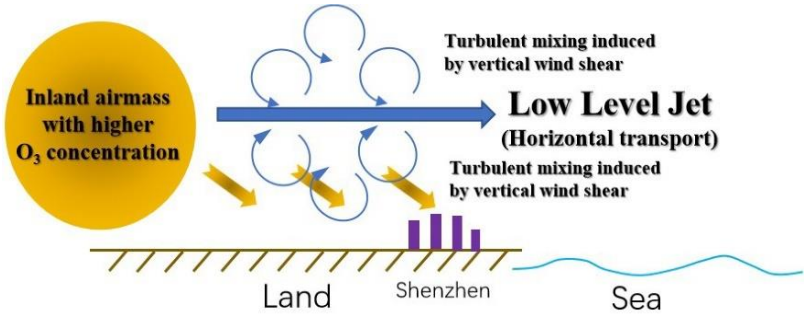

Figure 8. Conceptual model of nocturnal O_3 pollution under the land breeze over Shenzhen.

4. Conclusions

This study sought to reveal the long-term daily variation in O_3 concentrations in 2020, with a particular focus on nighttime O_3 pollution. Distinct nocturnal peaks were regularly observed around Shenzhen during the winter and spring, with monthly average daily variations showing a clear bimodal distribution. Further data analysis revealed that nighttime O_3 pollution occurred on 68 days in 2020 and was accompanied by a clear bimodal structure in the daily variation, with the maximum peak appearing from 12:00–14:00 during the day and the secondary peak mainly occurring from 23:00–03:00 at night.

Nocturnal O_3 pollution in Shenzhen was caused by two different types of weather conditions: high atmospheric stability, in favour of horizontal movement, and weak atmospheric stabilization, favouring vertical mixing. During the study period, 68 nights had secondary O_3 maximums that mainly occurred from 23:00 to 03:00 on the next day, with double peaks occasionally observed. Of the events, 16 cases can be explained by horizontal transport, while 22 can be explained by vertical mixing. We suggest that vertical mixing and horizontal transport are the main causes of the nocturnal secondary O_3 maximums. Under high atmospheric stability, O_3 pollution was closely related to the development of land breeze. For weak atmospheric stability, the analysis revealed no significant changes in wind direction (i.e., the absence of local and mesoscale weather systems). Instead, vertical mixing, which was closely related to LLJs, was identified as the major cause. LLJs occurred at night, with the wind speed at the centre reaching 15 m/s. The turbulent activity induced by the LLJs changed the structure of the residual layer and the stable boundary layer, leading to an increase in ground-level O_3 concentration.

The findings of this study confirm that nocturnal O_3 pollution often occurs during clear and stationary weather conditions in autumn and winter. Under such conditions, local and mesoscale wind field and vertical mixing will play an important role in urban wind circulation and pollution transport. The frequent occurrence of nocturnal O_3 pollution in Shenzhen requires particular attention from the government during their discussion on efforts related to pollution management.

Author Contributions: Conceptualization, H.Y. and L.L.; Data curation, C.L. and Y.H.; formal analysis, L.Z.; visualization, C.L.; methodology, L.L. and H.Y.; writing—original draft, H.Y.; writing—review and editing, P.-W.C. All authors have read and agreed to the published version of the manuscript.

Funding: This study was supported by the Guangdong Basic and Applied Basic Research Foundation (2019A1515012008), Guangdong Province Science and Technology Department Project (2019B121201002; 2021B1212050024), scientific research projects of Guangdong Provincial Meteorological Bureau (GRMC2020M29) and Science and Technology Innovation Team Plan of Guangdong Meteorological Bureau (GRMCTD202003).

Institutional Review Board Statement: Not applicable.

Informed Consent Statement: Not applicable.

Data Availability Statement: The authors are not authorized to share the data.

Acknowledgments: The authors are thankful for the data support from the European Centre for Medium-Range Weather Forecasts (ECMWF).

Conflicts of Interest: The authors declare no conflict of interest.

References

1. Zhang, Y.; Shao, K.; Tang, X.; Li, J. The Study of Urban Photochemical Smog Pollution in China. *Acta Sci. Nat. Univ. Pekinesis* **1998**, *34*, 392–400. (In Chinese)
2. Chen, P.; Quan, J.; Qiang, Z.; Tie, X.; Yang, G.; Xia, L.; Huang, M. Measurements of vertical and horizontal distributions of ozone over Beijing from 2007 to 2010. *Atmos. Environ.* **2013**, *74*, 37–44. [CrossRef]
3. Yang, C.; Yang, H.; Shu, G.; Wang, Z.; Xu, X.; Duan, X.; Kan, H. Alternative ozone metrics and daily mortality in Suzhou: The China Air Pollution and Health Effects Study. *Sci. Total Environ.* **2012**, *426*, 83–89. [CrossRef]
4. Huang, C.; Chen, C.H.; Li, L.; Cheng, Z.; Wang, H.L.; Huang, H.Y.; Streets, D.G.; Wang, Y.J.; Zhang, G.F.; Chen, Y.R. Emission inventory of anthropogenic air pollutants and VOC species in the Yangtze River Delta region, China. *Atmos. Chem. Phys.* **2011**, *11*, 4105–4120. [CrossRef]
5. Huang, J.; Zhou, C.; Lee, X.; Bao, Y.; Zheng, Y. The effects of rapid urbanization on the levels in tropospheric nitrogen dioxide and ozone over East China. *Atmos. Environ.* **2013**, *77*, 558–567. [CrossRef]
6. Aris, R.M.; Christian, D.; Hearne, P.Q.; Kerr, K.; Finkbeiner, W.E.; Balmes, J.R. Ozone-induced airway inflammation in human subjects as determined by airway lavage and biopsy. *Am. Rev. Respir. Dis.* **1993**, *148*, 1363–1372. [CrossRef] [PubMed]
7. Coleridge, J.C.; Coleridge, H.M.; Schelegle, E.S.; Green, J.F. Acute inhalation of ozone stimulates bronchial C-fibers and rapidly adapting receptors in dogs. *J. Appl. Physiol.* **1993**, *74*, 2345–2352. [CrossRef]
8. Feng, Z.; Kobayashi, K. Assessing the impacts of current and future concentrations of surface ozone on crop yield with meta-analysis. *Atmos. Environ.* **2009**, *43*, 1510–1519. [CrossRef]
9. Agyei, T.; Juráň, S.; Ofori-Amanfo, K.K.; Šigut, L.; Urban, O.; Marek, M.V. The impact of drought on total ozone flux in a mountain Norway spruce forest. *J. For. Sci.* **2020**, *66*, 280–287. [CrossRef]
10. Zhang, R.; Lei, W.; Tie, X.; Hess, P. Industrial emissions cause extreme urban ozone diurnal variability. *Proc. Natl. Acad. Sci. USA* **2004**, *101*, 6346–6350. [CrossRef]
11. Aneja, V.P.; Mathur, R.; Arya, S.P.; Li, Y.; Murray, G.C.; Manuszak, T.L. Coupling the vertical distribution of ozone in the atmospheric boundary layer. *Environ. Sci. Technol.* **2000**, *34*, 15–28. [CrossRef]
12. Corsmeier, U.; Kalthoff, N.; Kolle, O.; Kotzian, M.; Fiedler, F. Ozone concentration jump in the stable nocturnal boundary layer during a LLJ-event. *Atmos. Environ.* **1997**, *31*, 1977–1989. [CrossRef]
13. Coulter, R.L. A case study of turbulence in the stable nocturnal boundary layer. *Bound-Lay Meteorol.* **1990**, *52*, 75–91. [CrossRef]
14. Loeffler-Mang, M.; Kossmann, M.; Voegtlin, R.; Fiedler, F. Valley wind systems and their influence on nocturnal ozone concentrations. *KIT-Webmaster (SG)* **1997**, *70*, 1–14.
15. Jian, Z.; Rao, S.T.; Daggupaty, S.M. Meteorological Processes and Ozone Exceedances in the Northeastern United States during the 12–16 July 1995 Episode. *J. Appl. Meteorol.* **1998**, *37*, 776–789.
16. Jain, S.L.; Arya, B.C.; Kumar, A.; Ghude, S.D.; Kulkarni, P.S. Observational study of surface ozone at New Delhi, India. *Int. J. Remote Sens.* **2005**, *26*, 3515–3524. [CrossRef]
17. Chung, Y.S. Ground-Level Ozone and Regional Transport of Air Pollutants. *J. Appl. Meteorol. Clim.* **1977**, *16*, 1127–1136. [CrossRef]
18. Baumbach, G.; Vogt, U. Experimental determination of the effect of mountain-valley breeze circulation on air pollution in the vicinity of Freiburg. *Atmos. Environ.* **1999**, *33*, 4019–4027. [CrossRef]
19. Hu, X.M.; Doughty, D.C.; Sanchez, K.J.; Joseph, E.; Fuentes, J.D. Ozone variability in the atmospheric boundary layer in Maryland and its implications for vertical transport model. *Atmos. Environ.* **2012**, *46*, 354–364. [CrossRef]
20. Tong, N.; Leung, D.; Liu, C.H. A Review on Ozone Evolution and Its Relationship with Boundary Layer Characteristics in Urban Environments. *Water Air Soil Pollut.* **2011**, *214*, 13–36. [CrossRef]
21. Li, M.; Song, Y.; Mao, Z.; Liu, M.; Huang, X. Impacts of thermal circulations induced by urbanization on ozone formation in the Pearl River Delta region, China. *Atmos. Environ.* **2016**, *127*, 382–392. [CrossRef]
22. Yin, S.; Zheng, J.; Lu, Q.; Yuan, Z.; Huang, Z.; Zhong, L.; Lin, H. A refined 2010-based VOC emission inventory and its improvement on modeling regional ozone in the Pearl River Delta Region, China. *Sci. Total Environ.* **2015**, *514*, 426. [CrossRef]
23. Kaser, L.; Peron, A.; Graus, M.; Striednig, M.; Wohlfahrt, G.; Juráň, S.; Karl, T. Interannual variability of terpenoid emissions in an alpine city. *Atmos. Chem. Phys.* **2022**, *22*, 5603–5618. [CrossRef]
24. Yue, D.; Xie, M.; Zhou, Y.; Yuan, L.; Ou, Y. Influence of the New National Air Quality Standard on the Air Quality Assessment at the Regional Sites in the PRD Region. *Environ. Monit. China* **2013**, *29*, 38–42. (In Chinese)
25. Zhang, J.; Wang, T.; Chameides, W.L.; Cardelino, C. Ozone production and hydrocarbon reactivity in Hong Kong, Southern China. *Atmos. Chem. Phys.* **2007**, *6*, 557–573. [CrossRef]

26. Li, J.; Lu, K.; Lv, W.; Li, J.; Zhong, L.; Ou, Y.; Chen, D. Fast increasing of surface ozone concentrations in Pearl River Delta characterized by a regional air quality monitoring network during 2006–2011. *J. Environ. Sci.* **2014**, *26*, 23–36. [CrossRef]
27. Wang, T.; Xue, L.; Brimblecombe, P.; Lam, Y.F.; Li, L.; Zhang, L. Ozone pollution in China: A review of concentrations, meteorological influences, chemical precursors, and effects. *Sci. Total Environ.* **2017**, *575*, 1582–1596. [CrossRef]
28. Zhu, X.; Ma, Z.; Li, Z.; Wu, J.; Guo, H.; Yin, X.; Ma, X.; Qiao, L. Impacts of meteorological conditions on nocturnal surface ozone enhancement during the summertime in Beijing. *Atmos. Environ.* **2020**, *225*, 117368. [CrossRef]
29. He, C.; Lu, X.; Wang, H.; Wang, H.; Li, Y.; He, G.; He, Y.; Wang, Y.; Zhang, Y.; Liu, Y.; et al. Unexpected high frequency of nocturnal surface ozone enhancement events over China: Characteristics and mechanisms. *Atmos. Chem. Phys. Discuss.* 2022; *in review*. [CrossRef]
30. Shen, J.; Zhang, Y.; Wang, X.; Li, J.; Chen, H.; Liu, R.; Zhong, L.; Jiang, M.; Yue, D.; Chen, D.; et al. An ozone episode over the Pearl River Delta in October 2008. *Atmos. Environ.* **2015**, *122*, 852–863. [CrossRef]
31. Wang, H.; Wu, K.; Liu, Y.; Sheng, B.; Fan, S. Role of Heat Wave-Induced Biogenic VOC Enhancements in Persistent Ozone Episodes Formation in Pearl River Delta. *J. Geophys. Res. Atmos.* **2021**, *126*, e2020JD034317. [CrossRef]
32. Chen, Z.; Liu, J.; Cheng, X.; Yang, M.; Wang, H. Positive and negative influences of typhoons on tropospheric ozone over southern China. *Atmos. Chem. Phys.* **2021**, *21*, 16911–16923. [CrossRef]
33. Li, L.; Lu, C.; Chan, P.-W.; Zhang, X.; Yang, H.-L.; Lan, Z.-J.; Zhang, W.-H.; Liu, Y.-W.; Pan, L.; Zhang, L. Tower observed vertical distribution of $PM_{2.5}$, O_3 and NO_x in the Pearl River Delta. *Atmos. Environ.* **2020**, *220*, 117083. [CrossRef]
34. Hong-long, Y.; Yong, Z.; Lei, L.I.; Pak-wai, C.; Chao, L.U.; Li, Z. Characteristics of Aerosol Pollution Under Different Visibility Conditions in Winter in a Coastal Mega-City in China. *J. Trop. Meteorol.* **2020**, *26*, 231–238. [CrossRef]
35. Zurita, E.; Castro, M. A statistical analysis of mean hourly concentrations of surface ozone at Madrid (Spain). *Atmos. Environ.* **1983**, *17*, 2213–2220. [CrossRef]
36. Whiteman, C.D.; Bian, X.; Zhong, S. Low-level jet climatology from enhanced rawinsonde observations at a site in the southern Great Plains. *J. Appl. Meteor.* **1997**, *36*, 1363–1376. [CrossRef]
37. Stull, R.B. *An Introduction to Boundary Layer Meteorology: An Introduction to Boundary Layer Meteorology*; Springer: New York, NY, USA, 1988.
38. Kulkarni, P.S.; Bortoli, D.; Silva, A.M. Nocturnal surface ozone enhancement and trend over urban and suburban sites in Portugal. *Atmos. Environ.* **2013**, *71*, 251–259. [CrossRef]
39. Leung, Y.D.; Zhang, D.N. Characteristics of urban ozone level in Hong kong. *J. Environ. Sci.* **2001**, *13*, 1–7.
40. Saliba, N.A.; Moussa, S.; Salame, H.; El-Fadel, M. Variation of selected air quality indicators over the city of Beirut, Lebanon: Assessment of emission sources. *Atmos. Environ.* **2006**, *40*, 3263–3268. [CrossRef]
41. Kulkarni Pavan, S.; Bortoli, D.; Silva, A.M.; Reeves, C.E. Enhancements in nocturnal surface ozone at urban sites in the UK. *Environ. Sci. Pollut. Res.* **2015**, *22*, 20295–20305. [CrossRef]
42. Eliasson, I.; Thorsson, S.; Andersson-Skoeld, Y. Summer nocturnal ozone maxima in Gteborg, Sweden. *Atmos. Environ.* **2003**, *37*, 2615–2627. [CrossRef]
43. Ding, A.; Wang, T.; Zhao, M.; Wang, T.; Li, Z. Simulation of sea-land breezes and a discussion of their implications on the transport of air pollution during a multi-day ozone episode in the Pearl River Delta of China. *Atmos. Environ.* **2004**, *38*, 6737–6750. [CrossRef]